LETTER

# Geodesic acoustic mode (GAM) like oscillations and RMP effect in the STOR-M tokamak

IOP Publishing | International Atomic Energy Agency Nuclear Fusion

Nucl. Fusion **58** (2018) 024001 (6pp) https://doi.org/10.1088/1741-4326/aa9a4f

Letter

# Geodesic acoustic mode (GAM) like oscillations and RMP effect in the STOR-M tokamak

**Debjyoti Basu[1], Masaru Nakajima[1], A.V. Melnikov[2,3], David McColl[1], Akbar Rohollahi[1], Sayf Elgriw[1], Chijin Xiao[1] and Akira Hirose[1]**

[1] Plasma Physics Laboratory, University of Saskatchewan, Saskatoon, Canada
[2] NRC Kurchatov Institute, 123182, Moscow, Russian Federation
[3] National Research Nuclear University MEPhI, 115409, Moscow, Russian Federation

E-mail: debjyotibasu.basu@gmail.com and melnikov_07@yahoo.com

Received 8 September 2017, revised 25 October 2017
Accepted for publication 14 November 2017
Published 21 December 2017

**Abstract**

A new kind of quasi-coherent mode was observed in ohmic plasma in the STOR-M tokamak. It is featured with a clear solitary peak around 30–35 kHz in the power spectra of the ion saturation current $(I_{sat})$ of Langmuir probe as well as poloidal and toroidal mode numbers $(m = 1, n = 0)$ as per the prediction of conventional geodesic acoustic mode (GAM) theory. The dispersion relation of the mode is also similar to GAM and it also shows collisional damping. In contrast to conventional GAM, the floating potential $\phi$ of the observed GAM-like mode does not show similar symmetric poloidal and toroidal mode numbers $(m = 0, n = 0)$, but has $(m = 1, n = 1)$. The GAM-like mode has also a pronounced magnetic component with mixed poloidal modes ($m = 3$ and $m = 5; n = 1$), as observed by Mirnov coils. This mode is suppressed by the application of resonance magnetic perturbations.

Keywords: turbulent, tokamak, plasmas

(Some figures may appear in colour only in the online journal)

Zonal flow is a universal phenomenon present in turbulent systems, whether it is magnetically confined laboratory plasmas or space plasmas [1, 2]. Experimental [3] and theoretical [4, 5] studies of this phenomenon have become highly important to understand the transformation mechanism from turbulent or disordered state to ordered state like zonal flows [6]. Controlling energy/particle transport is crucial to achieve burning plasmas in reactor-grade tokamaks. Anomalous transport in tokamak plasmas arises due to small scale or turbulent fluctuations [2, 3]. On the other hand, the formation of zonal flows, created from electrostatic turbulent energy through a nonlinear process, helps to reduce cross-field transport. Also, recent gyrokinetic simulation shows that low frequency zonal flow can be formed by beta-induced Alfvén-eigenmode(BAE) [7] and BAE can exist in ohmic discharge tokamak plasma [8]. Zonal flow's formation is a self-organized process whose inherent physical nature is still not known.

In general, two types of zonal flow can be found in toroidal systems which are 'low frequency' residual zonal flow and 'high frequency' zonal flow or geodesic acoustic mode (GAM) which exist only in toroidal geometry. Conventional GAM is mainly characterized by (i) symmetric toroidal mode number $(n = 0)$ for both density fluctuations and potential/radial electric field fluctuations, (ii) symmetric poloidal mode number $(m = 0)$ only for potential/radial electric field fluctuations, but it is asymmetric in density fluctuation $(m = 1)$, (iii) strong domination of plasma potential fluctuations over density fluctuations, $e\delta\phi/T_e \gg \delta n/n$ [9]. Theoretically, mode frequency follows ion sound speed [9], so radially localized GAM frequency is expected. Extensive experimental studies on GAM

 

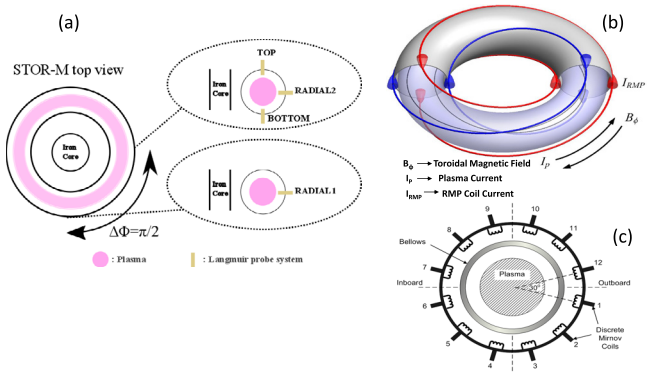


**Figure 1.** (*a*) Geometrical positions of four Langmuir probe systems in different geometrical locations, (*b*) RMP coil set, (*c*) a set of twelve Mirnov coils.

have been done in medium-to-large volume tokamaks and stellarators like TEXT [10], DIII-D [11], T-10 [12], etc [3].

The small tokamak STOR-M with circular cross-section has major and minor radii of 46 cm and 12 cm, respectively, with discharge duration around 30 ms. The plasma boundary is defined by an elliptical stainless steel poloidal limiter, placed in such a way that its internal major (13 cm) and minor (12 cm) radii have laid along horizontally and vertically. Three Langmuir probe systems(top, radial-2, bottom) were installed through the top, equatorial and bottom ports of the vessel in the same poloidal cross-section. A fourth one(radial-1) is placed equatorially, offset toroidally by 90° in a clockwise direction (top view) with respect to the other three sets. Each probe head has four pure tungsten probe tips of 1 mm diameter, placed on four corners of a square with side length of 2.25 mm. Each probe head is dedicated for measuring floating potential fluctuations ($\phi$), $I_{\rm sat}$ fluctuation and current–voltage(I–V) characteristics for electron temperature ($T_{\rm e}$) from the same plasma location. A set of Mirnov coils including twelve coils, placed poloidally with successive coil separation 30°, is dedicated to measuring magnetic fluctuations. These are located almost 135° apart in a clockwise toroidal direction (top view) with respect to the location of the group of three Langmuir probe systems. STOR-M is also equipped with a set of resonance magnetic perturbations (RMP) coils with $(m = 2; n = 1)$ [13]. The probe head and four probe systems' geometrical positions, Mirnov coils set and RMP coils are shown in figure 1.

The study was performed in plasmas with edge safety factor ($q_a$) $5.08 < q_a(= aB_{\rm T}/RB_{\rm p}) < 6.78$, toroidal magnetic field $B_{\rm T} = 0.65$ T, and plasma current 15 kA $< I_{\rm P} <$ 20 kA. Electron density ($n_{\rm e}$) averaged over central chord $2.5 \times 10^{19}$ m$^{-3}$ $< n_{\rm e} < 3.2 \times 10^{19}$ m$^{-3}$. A typical plasma discharge scenario is presented in figure 2. Top, radial-2, bottom, radial-1 Langmuir probe systems' heads were inserted into the plasma at a plasma radius of around 10 cm to measure $I_{\rm sat}$, $\phi$ and $T_{\rm e}$. Ideally, Langmuir probe tips should collect $I_{\rm sat}$,$\phi$ and I–V signals from the same magnetic flux surface. Locations of all probes at the same flux surface were verified by a similar amplitude of time traces of $I_{\rm sat}$ signals with tolerance of 10–12 mA, presented in figure 3(*e*).

A quasimonochromatic oscillation was noticed in $I_{\rm sat}$ signals from four probes. Figure 3 presents a typical GAM-like

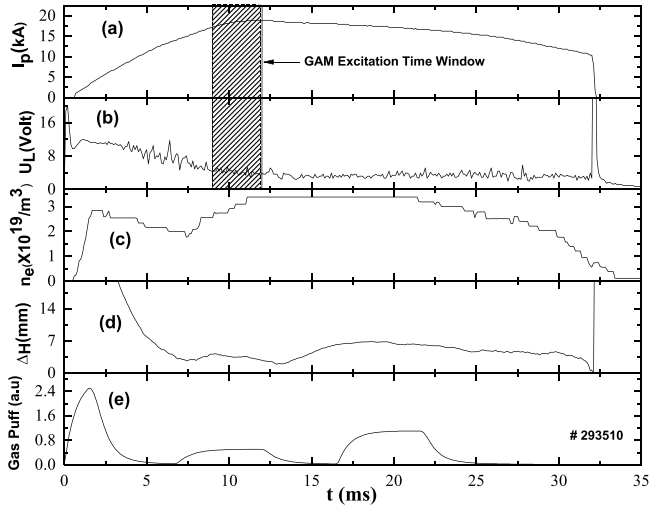


**Figure 2.** Temporal variation of (*a*) plasma current, (*b*) loop voltage, (*c*)line averaged density, (*d*) plasma horizontal position and (*e*) voltage waveform controlling gas puff.

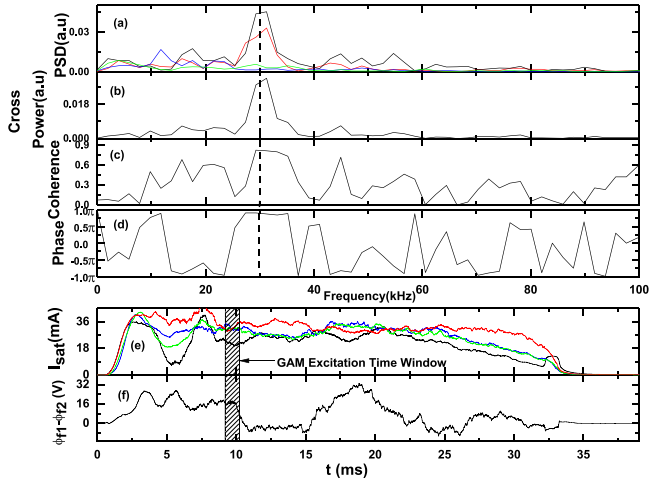


**Figure 3.** (*a*) Power spectral density of '$I_{\rm sat}$' signals of top (black line), bottom (red line), radial-2 (green line) and radial-1 (blue line) probes (the GAM-like frequency peak, marked by dashed line, is dominant over the power spectrum), (*b*) cross power between top and bottom GAM-like '$I_{\rm sat}$' signals, (*c*) coherence between top and bottom GAM-like '$I_{\rm sat}$' signals, (*d*) phase difference between top and bottom GAM-like '$I_{\rm sat}$' signals, (*e*) temporal variation of the '$I_{\rm sat}$' signal envelopes of top (black line), bottom (red line), radial 2 (green line) and radial 1 (blue line), (*f*) temporal envelope of two radially shifted $\phi$ signals difference.

behaviour of $I_{\rm sat}$ fluctuations and clearly illustrates that the power spectral density (PSD) of top and bottom $I_{\rm sat}$ fluctuations have a dominating solitary peak around 30 kHz but PSD of $I_{\rm sat}$ fluctuations from radial-1 and radial-2 have PSD at noise level. Clear indications of cross power, high coherence around 0.75 and phase difference around $0.9\pi$ have been observed in between top and bottom $I_{\rm sat}$ fluctuations. We consider that the equatorial plane has $\theta = 0$, then the top and bottom probes have corresponding $\theta = \pi/2$ and $\theta = -\pi/2$. So, phase difference is nearly $\pi$ between the top and bottom probes with nearly equal PSD of them as well as PSD at noise level of radial-2 density fluctuations, indicating $\sin\theta$ distribution of density fluctuations in the poloidal plane. Again, PSD at noise

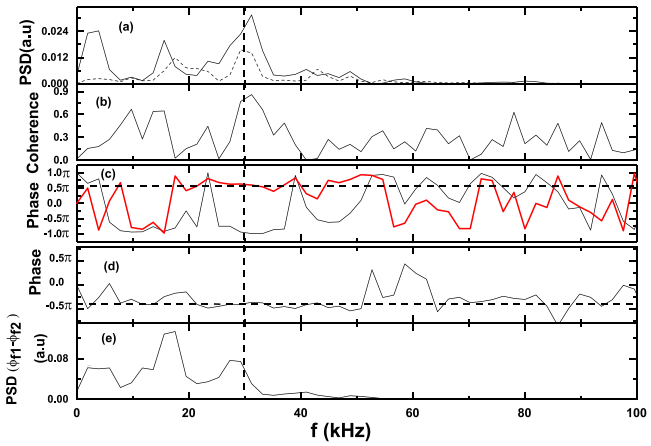


**Figure 4.** (*a*) power spectral density of top (black line) and bottom (dashed line) GAM-like $\phi$ signals, (*b*) coherence between top (solid line) and bottom $\phi$ signals, (*c*) poloidal phase difference between top and bottom GAM-like $\phi$ signals (black line) as well as toroidal phase difference between radial-1 and radial-2 GAM-like $\phi$ signals (red line) which indicate $(m = 1; n = 1)$, (*d*) phase difference between bottom $I_{sat}$ and bottom $\phi$, (*e*) PSD of two radially shifted $\phi$ signals difference.

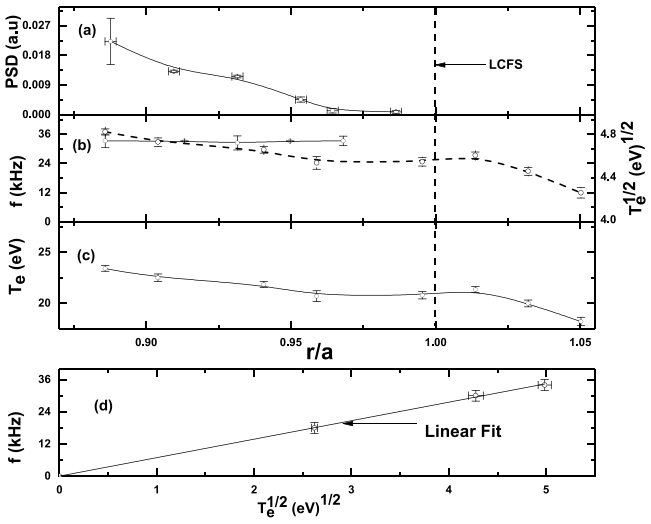


**Figure 5.** (*a*) Radial profile of the intensity of GAM-like frequency peak in the power spectral density of $I_{sat}$ signal, (*b*) frequency of GAM-like oscillations, and square root of electron temperature $(T_e^{1/2})$, (*c*) plasma electron temperature, (*d*) GAM-like oscillation frequency at $(r/a) = 0.83$ versus square root of electron temperature $(T_e^{1/2})$.

level of density fluctuations of radial-1 also supports $\sin\theta$ distribution of PSD in the poloidal direction since $\sin\theta = 0$ at $\theta = 0$. Also, the poloidal mode number of density fluctuations is $m = 1$, since the top and bottom probes have nearly $\pi$ phase difference. Numerically, it is difficult to derive the toroidal phase difference in between radial-1 and radial-2 density fluctuations since both have PSD at noise level. Since both PSD of radial-1 and radial-2 density fluctuations are at noise level following sinusoidal distribution in the poloidal direction, toroidal mode number $n = 0$ for the density perturbation is suggested. All these features are consistent with the theoretical expectation of GAM [9] ($n = 0$, $m = 1$, density perturbation) and experimental observation as well [14].

The mode number of $\phi$-signals does not show GAM-like behaviour as per theoretical expectation and experimental observations [14–16]. Figures 4(*a*)–(*c*) presents PSD, coherence and phase between top and bottom $\phi$. Top and bottom $\phi$ have almost equal PSD, high coherence but nearly $\pi$ phase difference which indicates poloidal mode number $m = 1$. Again, radial-1 and radial-2 $\phi$-signals have a phase difference of nearly $\pi/2$, presented in figure 4(*c*), which indicates toroidal mode number $n = 1$, since radial-1 and radial-2 probes are separated toroidally by $\pi/2$. So, $\phi$ mode number $(m = 1, n = 1)$ is in contrast to conventional GAM $(m = 0, n = 0)$. Interestingly, the phase difference between $I_{sat}$ and $\phi$ in the same geometrical locations always has nearly $0.5\pi$ at GAM-like frequency peak, presented in figure 4(*d*), which is consistent with GAM features [17]. The difference between two radial $\phi$ signals$(\delta\phi_r = \phi_{r1} - \phi r2)$, collected from radial-1$(\phi_{r1})$, radial-2$(\phi_{r2})$ which are not located exactly in the same magnetic surface, has a PSD peak around 30 kHz and provides an indication of radial electric field signal $(E_r)$. The frequency of the PSD peaks of both $I_{sat}$ and $\delta\phi_r$ is well matched. Figures 3(*f*) and 4(*e*) show time traces and PSD of $\delta\phi_r$ signal. Typically, GAM-like fluctuations are excited within a plasma discharge time window of around 9–12 ms, shown in figures 2(*a*) and (*b*). Its time duration varies from around 0.5–2 ms. In this typical example (figure 3), time duration is 9.2–10.2 ms.

The radial width of GAM-like oscillations is derived by measuring the magnitude of PSD peak of top $I_{sat}$ in different radial locations by moving top $I_{sat}$ radially through successive shots keeping other probes at constant positions. The outer boundary of the radial width is located at a normalized plasma radius $r/a = 0.97$ which is inside and close to the last closed magnetic flux surface(LCFS), shown in figure 5(*a*). It is consistent for limiter discharges [18]. However, the inner boundary of the radial width is undetermined because the top $I_{sat}$ could not be moved more than 9.75 cm $(r/a = 0.89)$ towards the plasma center, otherwise the plasma disrupts. The magnitude of PSD peak of top $I_{sat}$ increases rapidly towards the plasma center.

Here, an interesting feature is that the GAM-like oscillation frequency around 33 kHz remains constant over the investigated radial width though edge $T_e$ increases slowly towards the plasma center, as shown in figure 5(*c*) which is consistent with feature of global [19, 20] GAM-like mode, shown in figure 4(*b*). This is because $T_e$ changes around 3 eV over studied region extended from $\rho(r/a) = 0.97$ to 0.89. We obtain $\delta f = 2$ kHz using formulation $\delta f_{GAM} = \frac{1}{2\pi R}(\frac{1}{T_e m_i})^{1/2}\delta T_e$ at $T_e = 20$ eV and $\delta T_e = 3$ eV, which is in contrast with experimental outcomes.

The dispersion relation of GAM-like oscillation is verified by measuring oscillation frequency $(f)$ and corresponding $T_e$ at top $I_{sat}$ located at plasma radius 10 cm. A small variation of $T_e$ is obtained by slightly changing the gas puff as well as $I_p$ where $T_e$ is measured from Langmuir Probe I–V characteristics. The dispersion relation of conventional GAM theory is $f_{GAM} = \frac{c_s}{2\pi R}(2 + 1/q^2)^{1/2}$, where '$c_s$' and '$R$' stand

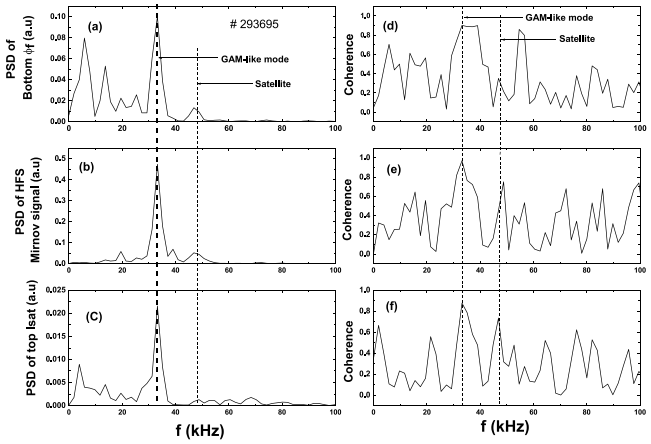


**Figure 6.** GAM-like peaks in the PSD of (*a*) floating potential signal $\phi$ in bottom probe, (*b*) Mirnov coil oscillations in high field side, (*c*) ion saturation current signal in top probe, coherence in between (*d*) bottom floating signal and high field side Mirnov oscillation, (*e*) top $I_{sat}$ and high field side Mirnov oscillation, (*f*) bottom floating signal and top $I_{sat}$. Remarkably, the higher-frequency satellite accompanies the main GAM-like peak.

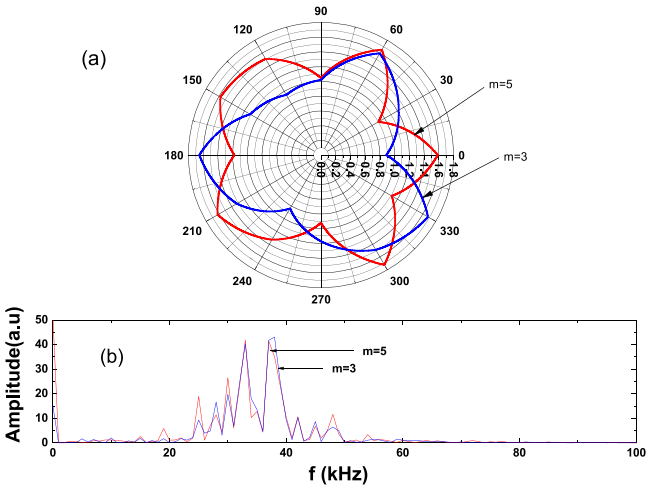


**Figure 7.** (*a*) Mode structure, (*b*) amplitude versus mode frequency.

for ion-acoustic speed and plasma major radius. The conventional GAM dispersion relation reduced to a simplified form is $f_{\rm GAM} = \frac{1}{\pi R}(\frac{T_e}{M_i})^{1/2}$ at $T_i = \frac{4}{7}T_e$ and neglecting $1/q^2$ term where $c_s = \sqrt{\frac{T_e+\frac{7}{4}T_i}{m_i}}$. Here, $T_i$ and $m_i$ present ion temperature and ion mass. We notice that the $f$ versus $T_e^{1/2}$ plot is well matched with the reduced form of the conventional GAM dispersion relation, shown in figure 5(*d*). We got GAM-like $f = 30$ kHz and 32 kHz at corresponding $T_e = 18$ eV and 21 eV.

On the other hand, the dispersion relation of beta induced Alfvén mode is [21] $f_{\rm EGAM/BAE} = (\frac{1}{2\pi R})(\frac{2T_i}{m_i})^{1/2}(\frac{7}{4}+\frac{T_e}{T_i})^{1/2}$. $f_{\rm BAE}$ and $f_{\rm GAM}$ merge for $T_e = \frac{4}{7}T_i$ because in this condition $f_{\rm BAE} = (\frac{1}{\pi R})(\frac{T_e}{m_i})^{1/2} = f_{\rm GAM}$. Again, according to the first hypothesis, [22] frequency scaling of global beta induced Alfvén eigenmode is $f_{\rm BAE} \leqslant f_{\rm TAE}/2q$, where $f_{\rm TAE} = \frac{B_T}{(4\pi qR)\sqrt{4\pi n_i m_i}}$ and we can well approximate $n_i m_i = n_e m_i$, where $n_i$ is ion density. For STOR-M, $f_{\rm TAE} = 225$ kHz at $B_T = 6500$ G, $R = 46$ cm, $q = 5$, $n_e = 5.10^{12}$ cm$^{-3}$, $m_i = 1.6.10^{-24}$ gm and $f_{\rm BAE} \leqslant 22.5$ kHz which is of the same order as the observed frequency range. It is clear that small tokamak STOR-M can support frequency range of BAE mode as well.

A typical example of a dominating GAM-like peak around 33.2 kHz with pronounced satellite peak around 46.8 kHz, present in all spectra, is shown in figure 6. Long range spatial correlation [23] of GAM-like $\phi$, $I_{sat}$, and Mirnov oscillations are examined in the poloidal plane by deriving the coherence between two parameters with all possible combinations of top $I_{sat}$, bottom $\phi$ and high field side(HFS) Mirnov signals as well as the PSD of three signals. These three signals have been selected from arbitrary positions. Clear frequency peaks around 33.2 kHz of PSD of bottom $\phi$, top $I_{sat}$ and HFS Mirnov signal have been observed in figures 6(*a*)–(*c*). Interestingly, coherence around $f = 33.2$ kHz has been observed between two parameters with all possible combinations of top $I_{sat}$, bottom $\phi$, HFS Mirnov signal and its magnitude varies from 0.85 to 0.9, shown in figures 6(*d*)–(*f*).

GAM-like Mirnov oscillations have mixture poloidal mode numbers $m = 3$ and $m = 5$ and toroidal mode number $n = 1$. Figure 7(*a*) shows poloidal mode structure $m = 3,5$ and figure 7(*b*) presents amplitude versus modes' frequency. Here, mode frequency has two strong peaks around 33.2 kHz and 37.5 kHz with other higher order weak peaks. Peaks around 33.2 kHz are matched with the GAM-like mode but the rest do not match. This example confirms that the GAM-like mode has the expected electromagnetic component [4, 5] which also follows conventional observations of magnetic component of turbulence driven GAM [14, 15, 25]. The higher-frequency satellite peak in all spectra resembles the earlier observation on tokamaks [14, 24]. A new important observation is the existence of a satellite peak in the magnetic component. The appearance of satellite peaks is very clear in some shots.

The typical behaviour of GAM-like Mirnov oscillations is shown in figure 8(*a*) which clearly indicates asymmetry in the magnitude of PSD of Mirnov oscillations in magnetic field surface towards the poloidal direction. The local plasma density has been varied by changing the gas puffing signal and corresponding top probe $I_{sat}$; HFS Mirnov signals have been recorded. Experimentally, the amplitude of the PSD peak of GAM-like $I_{sat}$ and HFS Mirnov oscillations decay with increasing local plasma density, as shown in figures 8(*b*) and (*c*). This reveals that the mode is damped through collision. Suitable mathematical functions have been tried to fit with these two empirical outcomes. It is observed that the amplitude of the PSD peak versus local plasma density of GAM-like $I_{sat}$ and HFS Mirnov fluctuations is well fitted with $0.95\exp(-0.7n_e)$ and $6.5\exp(-0.55n_e)$, respectively. The exponential decay of the PSD peak amplitude of GAM-like Mirnov oscillations is faster than GAM-like $I_{sat}$ oscillations.

Resonant magnetic perturbation (RMP [26]) was applied by the RMP system ($m = 2$,$n = 1$) during the plasma discharge time window of 7–10 ms which is just before the onset time of the GAM-like mode. The application of RMP has a noticeable effect on plasma parameters like $\phi_p$, $\phi$, $n_e$, $T_e$ and $P_e$ at the plasma edge of STOR-M discharge. In presence of RMP, spatial profiles of all those plasma parameters become steeper at the plasma edge compared to the reference discharge without

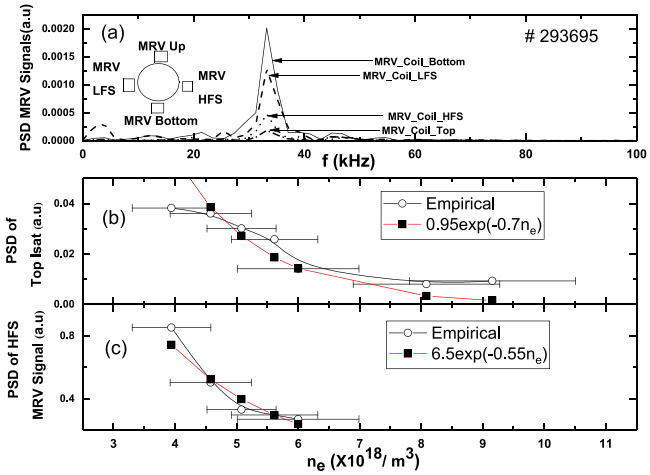


**Figure 8.** (*a*) PSD of Mirnov coils oscillations show GAM-like frequency peaks, (*b*) intensity of the GAM-like peak in PSD of $I_{sat}$ fluctuations versus local plasma density, (*c*) intensity of the GAM-like peak in PSD of HFS Mirnov coil oscillations versus local plasma density. (Open circle connected by black line shows the experimental profile, solid square connected by red line shows the exponential approximation).

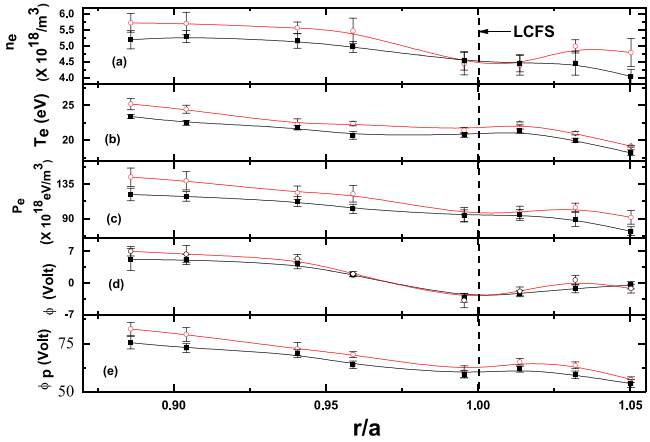


**Figure 9.** Spatial profiles of (*a*) plasma density, (*b*) electron temperature, (*c*) plasma electron pressure, (*d*) floating potential, (*e*) plasma potential, with RMP (open circle connected by red line) and without RMP (solid circle connected by black line).

RMP, as shown in figures 9(*a*)–(*e*), where RMP produced perturbing radial magnetic field around 0.0035 T at LCFS. Toroidal plasma flow is also modulated by the application of RMP in STOR-M discharge [13] and as a result magnetic fluctuations are suppressed. Apparently, this may be the possible reason for improved confinement due to the application of static RMP.

It was noticed that GAM like fluctuations in $I_{sat}$ and Mirnov probes are completely suppressed after applying magnetic perturbation where perturbing radial magnetic field is around 0.0035 T at LCFS. A typical example of GAM-like mode suppression in the presence of RMP is shown in figures 10(*a*)–(*f*). It is prominent from the figure that top and bottom GAM-like $I_{sat}$ fluctuations as well as GAM-like Mirnov coil fluctuations were completely suppressed.

It is clear from the experimental results that this mode, having a main frequency component and a high-frequency satellite, has an electromagnetic nature and seems to be a global

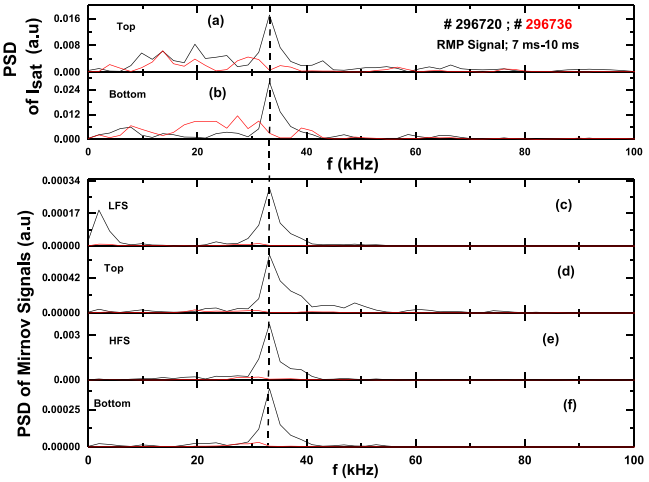


**Figure 10.** Effect of RMP on the GAM-like peak in Isat ((*a*), (*b*)) and Mirvov coils ((*c*)–(*g*)). PSD with RMP (red line), without RMP (black line).

mode with GAM frequency scaling with $T_e$. The considered mode is strongly dominant in the potential spectra since $(e\delta\phi/T_e) \approx 50(\delta n_e/n_e)$ which is like a conventional GAM characteristic. Again, similar to conventional GAM, floating potential fluctuations and density fluctuations in the same locations have a phase difference of $\pi/2$. Its density $(I_{sat})$ component also shows conventional GAM behaviour, but its potential component deviates from conventional GAM since it has $m = 1, n = 1$. So, the mode is not a conventional GAM but a sort of GAM-like mode. This mode experiences exponential damping through collision. Remarkably, the magnetic component decays faster than the $I_{sat}$ component. This mode is suppressed by RMP perturbation through magnetic interaction with the mode.

## Acknowledgments

We would like to acknowledge NSERC for supporting this work. We also would like to acknowledge machine workshops. Thanks go especially to Mr. Chomyshen and Mr. Toporowski in the machine workshops for their kind help and friendly approach when needed. The work of AVM was supported by Russian Science Foundation project 14-22-00193 and partly by the Competitiveness Programme of NRNU MEPhI.

## References

[1] Melnikov A.V. 2016 *Nat. Phys.* **12** 386
[2] Diamond P.H. *et al* 2005 *Plasma Phys. Control Fusion* **47** R35
[3] Fujisawa A. *et al* 2009 *Nucl. Fusion* **49** 013001
[4] Smolyakov A.I. *et al* 2010 *Nucl. Fusion* **50** 054002
[5] Bashir M.F. *et al* 2014 *Phys. Plasmas* **21** 082507
[6] Zhao K.J. *et al* 2006 *Phys. Rev. Lett.* **96** 255004
[7] Qiu Z. *et al* 2016 *Nucl. Fusion* **56** 106013
[8] Annibaldi S.V. *et al* 2007 *Plasma Phys. Control Fusion* **49** 475
[9] Winsor N. *et al* 1968 *Phys. Fluids* **11** 2448
[10] Schosh P. *et al* 2003 *Rev. Sci. Instrum.* **74** 1846
[11] McKee G. *et al* 2003 *Plasma Phys. Control Fusion* **45** A477

[12] Melnikov A.V. *et al* 2005 *Czech. J. Phys.* **55** 349
[13] Elgriw S. *et al* 2011 *Nucl. Fusion* **51** 113008
[14] Melnikov A.V. *et al* 2006 *Plasma Phys. Control Fusion* **48** S87
[15] de Meijere C.A. *et al* 2014 *Plasma Phys. Control Fusion* **56** 072001
[16] Wang G. *et al* 2013 *Phys. Plasmas* **20** 092501
[17] Melnikov A.V. 2015 *Nucl. Fusion* **55** 063001
[18] Simon P. *et al* 2016 *Plasma Phys. Control Fusion* **58** 045029
[19] Melnikov A.V. *et al* 2015 *JETP Lett.* **100** 555
[20] Ilgisonis V.I. *et al* 2014 *Plasma Phys. Control Fusion* **56** 035001
[21] Chen W. *et al* 2013 *Nucl. Fusion* **53** 113010
[22] Heidbrink W.W. *et al* 1999 *Phys. Plasmas* **6** 1147
[23] Melnikov A.V. 2015 *J. Phys.: Conf. Ser.* **591** 012003
[24] Kramer-Flecken A. *et al* 2007 Geodesic acoustic mode-radial extension and interaction with magnetic islands *34th EPS Conf. (Warsaw, 2-6 July 2007)* **31F** p 427
[25] Bulanin V.V. *et al* 2016 *Plasma Phys. Control Fusion* **58** 045006
[26] Seidl J. *et al* 2017 *Nucl. Fusion* **57** 126048